This article has been accepted for publication in IEEE Transactions on Radar Systems. This is the author's version which has not been fully edited and content may change prior to final publication. Citation information: DOI 10.1109/TRS.2024.3387950

A Modified Kirchhoff Migration for Microwave Imaging in Superluminal Propagation Region

Fatemeh Modares Sabzevari, *Student Member, IEEE,* Robert S. C. Winter, *Student Member, IEEE,* and Karumudi Rambabu , *Member, IEEE*

***Abstract*—Microwave imaging has been developed recently and is used in many applications. Kirchhoff's migration technique is one of the most popular methods to recover the geometric info of any inaccessible target from raw data. The conventional Kirchhoff's migration assumes a uniform propagation velocity in the far-field region of the transceiver, i.e., the antenna. In the near-field region of the antenna, the pulse propagation happens at a significantly greater speed compared to the far-field region. The propagation speed of the pulse depends on the antenna dimensions and varies as a function of the distance and angle of the antenna in a non-linear manner. This non-linearity causes non-focused images. In this work, a modified Kirchhoff's migration method is proposed to take into account the non-uniformity of the propagation speed. Then, the proposed method is verified through several simulations and experiments and it is shown that the modified Kirchhoff's migration results in focused images in the near-field region.**

***Index Terms*—Near-field imaging, Kirchhoff's migration, synthetic aperture radar (SAR), ultra-wideband (UWB) technology.**

I. Introduction

MICROWAVE imaging is a nondestructive technique to acquire information on inaccessible objects in the ground, behind the wall, etc [1]–[5]. The data acquisition can be performed either in the time-domain or the frequency-domain [6]. The raw data is then post-processed and converted to the spatial domain to form a focused image of the Region of Interest (ROI). The process of converting the raw time-space or frequency-space data to a 2D or 3D image is called migration [7].

In the literature, various migration techniques are available, which can be classified into i) Diffraction summation, (ii) Phase-shift migration, iii) Kirchhoff's migration, vi) Frequency-wavenumber (w-k) migration, and v) Back-projection based migration [7]–[9]. Diffraction summation and phase-shift migration are the most popular algorithms thanks to their easy implementation. However, they are not well-suited for high-quality imaging applications. This inaccuracy originates from the fact that these methods are not developed based on rigorous wave equations [8]. Kirchhoff's and frequency-wavenumber migration techniques are rooted in wave equations. The goal of Kirchhoff's migration is to find a solution to the scalar wave equation, and it exploits Kirchhoff's integral theorem [10]. Kirchhoff's migration technique can provide higher-quality images compared to diffraction summation. The frequency wave number is also derived from the scalar wave equation, and the image reconstruction is done in the spatial Fourier domain. Frequency wave number migration is a more computationally efficient method than other time-domain integral techniques, i.e., Kirchhoff's migration. However, the data acquisition must be in uniformly spaced transceiver positions, which may limit the usage of this technique [8]. The back-projection based migration techniques are developed on the tomographic principles. Unlike the frequency-wave number migration, the back-projection algorithm does not need an evenly-spaced data acquisition. Another advantage of this migration is that the image reconstruction can be started before the data capture is entirely completed, making this technique suitable for real-time applications. However, back-projection techniques migrate a single spike to an arc that causes the undesired sidelobe in the reconstructed image [11].

In ultra wide-band (UWB) microwave imaging, the ROI is illuminated by a series of short pulses and the transient response is recorded. Then the space-time domain data are transformed into a 2D or 3D image by one of the aforementioned migration techniques. Kirchhoff's migration provides a focused image with significantly higher quality and is more computationally efficient. For these reasons, Kirchhoff's migration is the most popular focusing technique for UWB radar SAR imaging [8], [12].

In many practical applications, the target is in the antenna's near field. Many researchers developed near-field migration techniques [13]–[17]. However, none of them has addressed the time-domain Kirchhoff's migration in the near region of the antenna. In [18], the propagation speed of the signal in the medium is considered to be constant. This approximation is not valid in the near-field and Fresnel region of the antenna [19], [20] and deteriorates the reconstructed image created by Kirchhoff's migration.

In this paper, a modified Kirchhoff's migration technique for the near-field region is proposed, and the non-uniformity of the pulse propagation speed is compensated. Then, the modified technique is validated through several simulations and experimental scenarios. The proposed modified Kirchhoff's migration is applied to Circular SAR (CSAR) and Linear SAR (LSAR) techniques, and the reconstructed images are compared to the conventional Kirchhoff's technique.

This work was supported by the Natural Sciences and Engineering Research Council of Canada (NSERC) under CRD Grants and Discovery Grants.

F. Modares Sabzevari,Robert S. C. Winter, and K. Rambabu are with the Electrical and Computer Engineering Department, University of Alberta, Edmonton, AB T6G 2V4, Canada (e-mail: modaress@ualberta.ca; and rambabu@ualberta.ca).

Authorized licensed use limited to: University College London. Downloaded on April 24,2024 at 17:59:49 UTC from IEEE Xplore. Restrictions apply.
© 2024 IEEE. Personal use is permitted, but republication/redistribution requires IEEE permission. See https://www.ieee.org/publications/rights/index.html for more information.

This article has been accepted for publication in IEEE Transactions on Radar Systems. This is the author's version which has not been fully edited and content may change prior to final publication. Citation information: DOI 10.1109/TRS.2024.3387950

This paper is organized as follows. The methodology and formulation of the proposed technique are described in Section II. Section III is devoted to the simulation validation. Experimental validation is presented in Section IV. Section V summarizes the results and concludes the paper.

II. Modified Kirchhoff's Migration Formulation

The scalar wave equation in a lossless medium can be written as [12]

$$\nabla^2\Psi(\vec{r},t) - \frac{1}{{v_m}^2}\frac{\partial^2\Psi(\vec{r},t)}{\partial t^2} = -f(\vec{r},t) \tag{1}$$

where Ψ is the wave amplitude, v_m is the propagation speed, and f is the source function of the wave evaluated at position $\vec{r}$ and time t. In a source-free ROI, i.e., $f(\vec{r},t) = 0$, Green's theorem can be applied to solve the (1).

$$\Psi(\vec{r},t) = -\frac{1}{4\pi}\int_0^\infty \int \Big(\Psi\frac{\partial G}{\partial n'} - G\frac{\partial \Psi}{\partial n'}\Big)\, dA'\, dt' \tag{2}$$

(2) is known as Kirchhoff's integral theorem, where n' and G are the unit normal vector to the surface and Green's function, respectively. In an isotropic medium [21]

$$\frac{\partial G}{\partial n'} = 0 \tag{3}$$

It should be noted that the wave amplitude or Ψ can be acquired from the measurements. The solution to the above equation is

$$\Psi(\vec{r},t) = \iint_V \Big(\frac{cos\theta}{v_m\ r}\ \frac{\partial}{\partial t}\Psi(\vec{r},t\ -\frac{r}{v_m})\Big)\, d\phi\, d\rho \tag{4}$$

where θ is the angle of the incident wave to the propagation axis. i.e., $z\ .\ cos\theta$ can be calculated as follows

$$cos\theta = \frac{z - z_t}{r} \tag{5}$$

where (x_t, y_t, z_t) and (x, y, z) are the coordinates of the observation point and receiver, respectively. The above integral equation with N number of receiver positions can be approximated with the following

$$\Psi(\vec{r},t) = \sum_{i=1}^{N}\Big(\frac{cos\theta_i}{v_m\ r_i}\ \frac{\partial}{\partial t}\Psi(\vec{r},t\ -\frac{r_i}{v_m})\Big) \tag{6}$$

where r_i is the Euclidean distance between the observation point and the receiver position.

To reconstruct the image of ROI, each point of the imaging area can be considered as a point scatterer and the goal is to retrieve the wave amplitude at the time the wavefront interacts with that point. For all the receiver apertures, the above procedure is carried out and an image value is calculated for each observation point by aggregating the wave amplitudes. As mentioned in (4), the propagation velocity of the wavefront is needed for the reconstruction. In the far-field region of the antenna, the group velocity can be acquired as follows

$$v_m = c = \frac{c_0}{\sqrt{\varepsilon_r}} \tag{7}$$

where c and ε_r are the speed of the light in the medium, and the dielectric constant of the propagation medium, respectively. However, in the near-field region of the antenna, the group velocity is not equal to c_0. In [13], [20], is shown that the pulse propagation speed is a function of the distance and angle in the near-field propagation region. To compensate for the variable propagation speed for Kirchhoff's Migration, the modified Kirchhoff's is proposed as:

$$\Psi(\vec{r},t) = \iint_V \Big(\frac{cos\theta}{v_m(\phi,\rho)\ r}\ \frac{\partial}{\partial t}\Psi(\vec{r},t\ -\frac{r}{v_m(\phi,\rho)})\Big)\, d\phi\, d\rho \tag{8}$$

where the propagation velocity i.e., v_m is a function of the observation point. This is significantly essential for any near-field microwave imaging since the pulse propagation speed can escalate up to 6 times for a 6-GHz dipole antenna as we move from the far-field region to a few centimeters [13]. In order to verify the proposed modified Kirchhoff's migration, the discrete version of the (8) is presented as follows

$$\Psi(\vec{r},t) = \sum_{i=1}^{N}\Big(\frac{cos\theta_i}{v_m(\phi,\rho)\ r_i}\ \frac{\partial}{\partial t}\Psi(\vec{r},t\ -\frac{r_i}{v_m(\phi,\rho)})\Big) \tag{9}$$

Note that v_m should be measured beforehand the data collection for SAR imaging; different transceivers demonstrate various pulse peak velocities profiles. In this work, miniaturized Vivaldi antennas, as shown in Fig. 1a, are used as a transceiver, and the pulse propagation velocity as a function of distance and angle i.e., $v_m(\phi,\rho)$ is employed to reconstruct the image. To measure the velocity profile, the Vivaldi transceiver is set up as shown in Fig.1b, and metal pins are placed at different angles and distances of the transceiver, i.e., $r_i = 1, 2, 3, \ldots, 15\ cm$. Then, the actual time that it takes for the pulse peak to be transmitted, reflected back, and received by the transceiver is measured by a sampling oscilloscope. Fig. 1c illustrates the measured pulse-peak velocity of the miniaturized Vivaldi antenna transceiver as a function of distance and angle. Note that pulse-peak velocity measurement is done in air, i.e., $\varepsilon_r = 1$. Also, the propagation medium for all simulations and measurements is air.

III. Simulation Validation

In order to verify the proposed modified Kirchhoff migration, several imaging scenarios are conducted in the near-field region of the antenna. In all cases, the reconstructed images by conventional and modified Kirchhoff migration techniques are presented side by side for comparison. The SAR technique is exploited to sample the wave amplitudes in the spatial domain. To mitigate the effect of surrounding objects, the calibration procedure is done as follows

$$s_{cal,i} = s_{raw,i} - s_{am,i}, \qquad i = 1, 2, ..., N \tag{10}$$

where $s_{cal,i}$, $s_{raw,i}$, and $s_{am,i}$ are the calibrated signal, the raw signal, and the ambient signal of the aperture i, respectively. Please note that the ambient signal comprises the combined effects of the transmitter and receiver antenna's mutual coupling, radar fixture, and nearby objects. However,

Authorized licensed use limited to: University College London. Downloaded on April 24,2024 at 17:59:49 UTC from IEEE Xplore. Restrictions apply.
© 2024 IEEE. Personal use is permitted, but republication/redistribution requires IEEE permission. See https://www.ieee.org/publications/rights/index.html for more information.

This article has been accepted for publication in IEEE Transactions on Radar Systems. This is the author's version which has not been fully edited and content may change prior to final publication. Citation information: DOI 10.1109/TRS.2024.3387950

in the simulation validations, the ambient signal specifically refers to the mutual coupling between the transmitter and receiver. Two sets of experiments are conducted, including CSAR and LSAR configurations. Note that all the images are presented in a log scale to highlight the distinction of the targets with respect to the background.

A. Modified Kirchhoff Migration for the CSAR Near-Field Imaging

The simulation setup is a three-point target scenario, as shown in Fig. 2a. The distance between the three targets is 2.83, 2.83, and 4 cm. The excitation signal is a second derivative Gaussian pulse with a full width at half maximum (FWHM) of 48 ps which corresponds to a -10 dB bandwidth of 8.66 GHz. The data is collected circularly in 18 different apertures, as it is marked with green plus markers in Fig. 2a. The calibrated signal along the apertures is illustrated in Fig. 2b. The focused images using the conventional and modified Kirchhoff algorithm are shown in Fig. 2c, and Fig. 2d, respectively. Both images are normalized and the same color map is used for the comparison purpose. As seen, the conventional Kirchhoff migration is not successful in focusing the image of the targets due to the non-uniform velocity of the propagation. However, the proposed modified Kirchhoff's algorithm is able to focus the right point target since the variable velocity profile compensates for the near-field region non-linearity.

Note that the expected resolution of the CSAR can be calculated as [6]:

$$\Delta_R = \frac{c}{3BW\sqrt{\varepsilon_r}} = \frac{3\times10^8}{3\times8.66\times10^9\times\sqrt{1}} = 1.15\ cm \quad (11)$$

The targets' separation in all CSAR simulation and experiments are greater than 1.15 cm, hence it is expected to resolve the targets successfully.

IV. Experimental Validation

In all conducted experiments, miniaturized Vivaldi antennas were employed as the radar transmitter and receiver, exhibiting a gain of 5-8 dBi across the frequency range of 3.2-15 GHz. The transmitted signal is a second derivative Gaussian pulse with a FWHM of 48 ps which corresponds to a bandwidth of 8.66 GHz. This pulse is generated by AVTECH AVP-3SA-C with a chain of 10-V steps and a pulse repetition frequency (PRF) of 1 MHz. The receiver antenna is connected to the high-frequency sampling oscilloscope. To increase the received signal SNR, a 64-time averaging is performed in the sampling oscilloscope. The number of time-domain samples for each aperture is 4050. The recorded data are then interpolated to 10000 data points. In addition, a moving average filter is applied to reduce the measurement noise.

A. Experiment 1, Circular SAR Near Field Imaging

First, a three-target CSAR scenario experiment is conducted. Three metal nails with a height of 15 cm and radius of 3.75 mm are adhered to a rotating wooden board. The transceiver

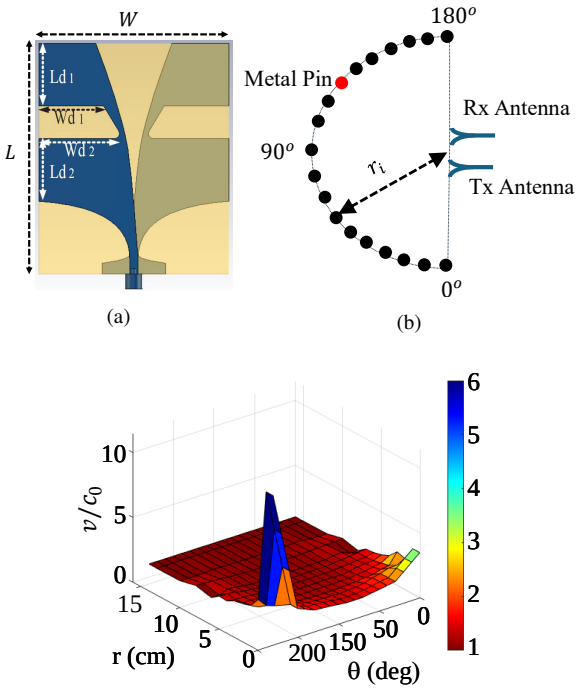

Fig. 1. a) Miniaturized Vivaldi antenna: L = 46mm, W = 36mm, Ld1 = 12.5mm, Ld2 = 12.5mm, Wd1 = 12.3mm, Wd2 = 14.3mm. b) Experimental setup to measure pulse-peak velocity. c) Measured propagation velocity of the miniaturized Vivaldi transceiver in the near-field region.

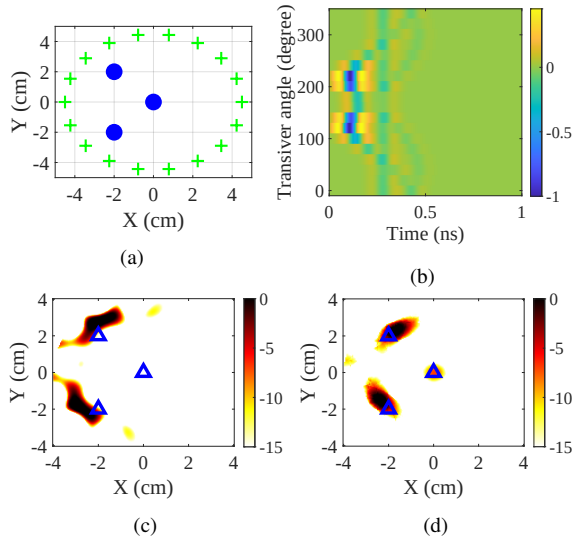

Fig. 2. CSAR simulation scenario. a) Simulation setup, b) calibrated data, c) reconstructed image by conventional Kirchhoff's migration, d) reconstructed image by the proposed Kirchhoff's technique.

radius is 2 cm and the data is collected in 36 positions with an increment of 10 deg. The reconstructed positive [22] and real images by the conventional Kirchhoff migration and the modified Kirchhoff migration are illustrated in Fig. 3 b-e. All the images are normalized and shown on the same scale for the purpose of comparison. By comparing Fig. 3c and

Authorized licensed use limited to: University College London. Downloaded on April 24,2024 at 17:59:49 UTC from IEEE Xplore. Restrictions apply.
© 2024 IEEE. Personal use is permitted, but republication/redistribution requires IEEE permission. See https://www.ieee.org/publications/rights/index.html for more information.

This article has been accepted for publication in IEEE Transactions on Radar Systems. This is the author's version which has not been fully edited and content may change prior to final publication. Citation information: DOI 10.1109/TRS.2024.3387950

3b, it is observed that the conventional Kirchhoff's algorithm represents each point target as multiple point targets, especially the middle bottom target. While the proposed modified Kirchhoff's technique successfully maps the spatial-time data into one single focused point target with true positions.

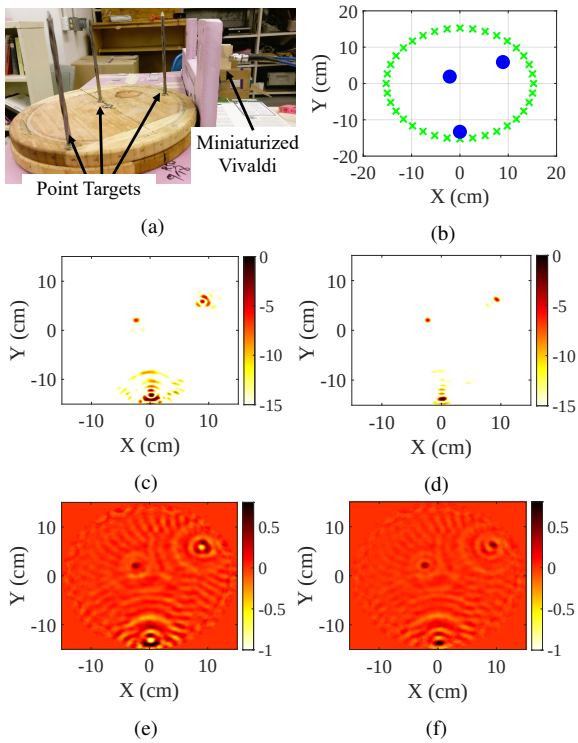

Fig. 3. a) CSAR Experimental setup, b) schematic setup (Top view). Reconstructed positive image by c) conventional Kirchhoff's migration, d) proposed Kirchhoff's technique. e) Reconstructed real image by conventional Kirchhoff's migration, and f) proposed Kirchhoff's technique.

B. Experiment 2, Circular SAR Near Field Imaging

The second experiment is a four-target scenario which is emulated by gluing four metal nails in a tilted square shape, as shown in Fig. 4a. The square side is 2 cm and the transceiver radius is 5 cm. The total number of aperture is 36 with a 10 deg increment to cover 360 deg.
The spatial-time domain collected data is exploited to focus 2D image by conventional and proposed modified Kirchhoff's migration technique. The reconstructed conventional image using c_0 is shown in Fig. 4b, and the reconstructed image using the specified pulse-peak velocity is shown in Fig. 4c. The reconstructed image using the characteristic speeds clearly focuses four targets; whereas, in the conventional Kirchhoff image, the four targets are completely merged together.

C. Experiment 3, Linear SAR Near Field Imaging

In this subsection, the LSAR configuration is used to collect data, where the antenna apertures are aligned in a line. The total aperture length is 41 cm with a spacing of 1 cm, as illustrated in Fig. 5a. The targets are two metal pins that are glued to a wooden board with the cartesian coordinates of

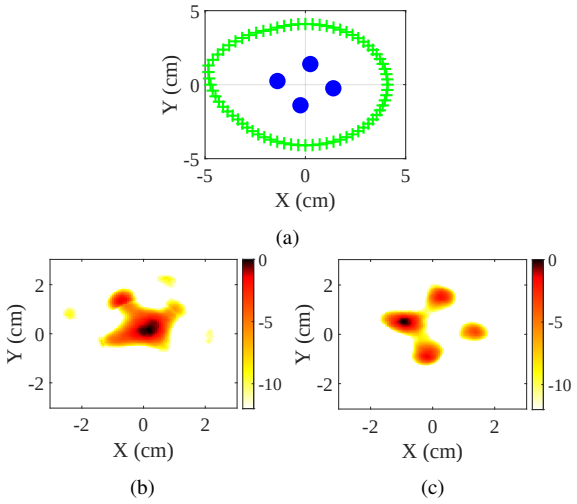

Fig. 4. CSAR Experiment with four nails. a) Experiment setup. b) Reconstructed image by conventional Kirchhoff's migration. c) Reconstructed image by the proposed Kirchhoff technique.

$(3.7, 1.4)$ cm and $(12.7, 2.3)$ cm, as shown with blue dots in Fig. 5a. The expected cross-range resolution can be estimated as [23]:

$$\delta_x \cong \frac{\lambda_c R_0}{2L_x} \tag{12}$$

where L_x, R_0, and λ_c are the synthetic aperture length, the antenna distance to the target scene, and the wavelength at the center frequency, respectively. Hence the expected cross-range resolution is:

$$R_0 = 2.3\ cm, f_c = 5.83\ GHz \Rightarrow \delta_x \cong 7.5\ mm \tag{13}$$

The reconstructed image using conventional Kirchhoff and the one using the proposed modified Kirchhoff are shown in Fig. 5b and 5c, respectively. As can be seen, the conventional Kirchhoff's migration image fails to focus the target, particularly the left nail, which is very close to the transceiver antenna, and the propagation speed is more deviated from c_0. The modified Kirchhoff's technique, which takes into account the variable propagation speeds, focuses the targets with correct positions.

D. Experiment 4, Linear SAR Near Field Imaging

The last experiment is conducted to emulate UWB SAR technology for oil well perforation [1]. The transceiver configuration is monostatic, with a spacing of 0.5 cm between the Tx and Rx antenna. Three holes with a radius of 1.27 cm are cut from a metal sheet. Then, the metal sheet is placed at a distance of 1 cm below the transceiver. The total antenna aperture length is 50 cm, with a 1 cm distance between each aperture. The experiment setup details are illustrated in Fig. 6a. The target is in the near-field of the transceiver antenna. In this experiment, the expected cross-range resolution can be estimated using 12:

$$R_0 = 1\ cm, f_c = 5.83 GHz \Rightarrow \delta_x \cong 7.3\ mm \tag{14}$$

The conventional modified Kirchhoff's migration is applied to reconstruct the ROI. Then a threshold of 0.6 is applied, and

Authorized licensed use limited to: University College London. Downloaded on April 24,2024 at 17:59:49 UTC from IEEE Xplore. Restrictions apply.
© 2024 IEEE. Personal use is permitted, but republication/redistribution requires IEEE permission. See https://www.ieee.org/publications/rights/index.html for more information.

This article has been accepted for publication in IEEE Transactions on Radar Systems. This is the author's version which has not been fully edited and content may change prior to final publication. Citation information: DOI 10.1109/TRS.2024.3387950

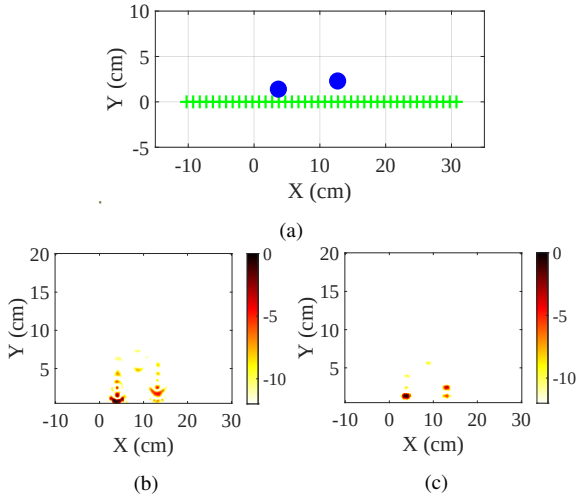

Fig. 5. Linear SAR Experiment. a) Experimental setup. b) Reconstructed image by conventional Kirchhoff's migration, c) reconstructed image by the proposed Kirchhoff's technique.

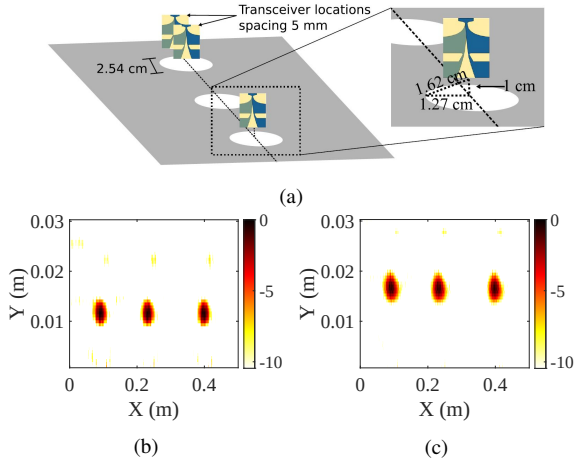

Fig. 6. Linear SAR Experiment. a) Experimental setup. b) Reconstructed image by conventional Kirchhoff's migration, c) reconstructed image by the proposed Kirchhoff's technique.

the image is shown in Fig 6b. Then the space-time domain data is fed to the proposed modified Kirchhoff's, and the same threshold is applied. The final image is illustrated in Fig. 6c. The modified Kirchhoff's migration technique produced the images of three holes in their true position; however, the conventional Kirchhoff's technique focuses the energy in the wrong positions.

V. Conclusion

This paper presents a novel focusing algorithm based on Kirchhoff's migration technique to compensate for the superluminal group velocity in the near-field region of the antenna. The proposed modified Kirchhoff migration is applied to various scenarios, including CSAR and LSAR. First, a CSAR data acquisition is generated in the simulator, and the image is reconstructed using different target scenarios, and the image of the ROI is reconstructed using the conventional Kirchhoff and the proposed modified Kirchhoff's migration. It is shown that the conventional Kirchhoff's migration fails to focus the energy on at least one target among all the experiments. In LSAR experiments, the modified Kirchhoff algorithm generates the image with the correct position and dimension, whereas in the image reconstructed by conventional Kirchhoff, the position of the targets is not matched to the true location. The proposed algorithm can be effectively used for near-field radar imaging.

Acknowledgment

The authors would like to thank Dr. R. Feghhi for providing the pulse generator used in some of the experiments.

References

[1] D. Oloumi and K. Rambabu, "Metal-cased oil well inspection using near-field uwb radar imaging," *IEEE Transactions on Geoscience and Remote Sensing*, vol. 56, no. 10, pp. 5884–5892, 2018.

[2] F. M. Sabzevari, A. E.-C. Tan, and K. Rambabu, "Real-time permittivity extraction based on ultra-wideband impulse radar and genetic algorithm for tunnel construction operations," *IEEE Sensors Journal*, 2023.

[3] R. Feghhi, R. S. Winter, F. M. Sabzevari, and K. Rambabu, "Design of a low-cost uwb time-domain radar system for subcentimeter image resolution," *IEEE Transactions on Microwave Theory and Techniques*, vol. 70, no. 7, pp. 3617–3628, 2022.

[4] A. Karimov, R. Feghhi, F. M. Sabzevari, R. S. Winter, R. Fedosejevs, and K. Rambabu, "Design and development of a high-power pulse transmitter for underground environmental perception," *IEEE Transactions on Microwave Theory and Techniques*, vol. 70, no. 5, pp. 2891–2903, 2022.

[5] M. Alesheikh, R. Feghhi, F. M. Sabzevari, A. Karimov, M. Hossain, and K. Rambabu, "Design of a high-power gaussian pulse transmitter for sensing and imaging of buried objects," *IEEE Sensors Journal*, vol. 22, no. 1, pp. 279–287, 2021.

[6] F. M. Sabzevari, R. S. C. Winter, D. Oloumi, and K. Rambabu, "A microwave sensing and imaging method for multiphase flow metering of crude oil pipes," *IEEE Journal of Selected Topics in Applied Earth Observations and Remote Sensing*, vol. 13, pp. 1286–1297, 2020.

[7] C. Özdemir, Ş. Demirci, E. Yiğit, and B. Yilmaz, "A review on migration methods in b-scan ground penetrating radar imaging," *Mathematical Problems in Engineering*, vol. 2014, 2014.

[8] X. Zhuge, T. Savelyev, A. Yarovoy, L. Ligthart, and B. Levitas, "Comparison of different migration techniques for uwb short-range imaging," in *2009 European Radar Conference (EuRAD)*, pp. 184–187, 2009.

[9] Y. Yue, Y. Liu, Y. Ye, Y. Wo, and Z. Qian, "Least-squares kirchhoff depth migration with fast point-spread-function computation," *IEEE Transactions on Geoscience and Remote Sensing*, vol. 61, pp. 1–10, 2023.

[10] Ö. Yilmaz, *Seismic data analysis: Processing, inversion, and interpretation of seismic data*. Society of exploration geophysicists, 2001.

[11] X. Zhuge, T. Savelyev, A. G. Yarovoy, and L. Ligthart, "Uwb array-based radar imaging using modified kirchhoff migration," in *2008 IEEE International Conference on Ultra-Wideband*, vol. 3, pp. 175–178, IEEE, 2008.

[12] T. Sakamoto, T. Sato, P. J. Aubry, and A. G. Yarovoy, "Ultra-wideband radar imaging using a hybrid of kirchhoff migration and stolt fk migration with an inverse boundary scattering transform," *IEEE Transactions on Antennas and Propagation*, vol. 63, no. 8, pp. 3502–3512, 2015.

[13] R. S. C. Winter, D. Oloumi, and K. Rambabu, "Uwb sensor characterization for radar sensing and imaging in superluminal propagation regions," *IEEE Transactions on Microwave Theory and Techniques*, vol. 69, no. 1, pp. 297–307, 2021.

[14] S. Li, S. Wang, M. G. Amin, and G. Zhao, "Efficient near-field imaging using cylindrical mimo arrays," *IEEE Transactions on Aerospace and Electronic Systems*, vol. 57, no. 6, pp. 3648–3660, 2021.

[15] B. Liang, X. Shang, X. Zhuge, and J. Miao, "Accurate near-field millimeter-wave imaging of concave objects—a case study of dihedral structures under monostatic array configurations," *IEEE Transactions on Geoscience and Remote Sensing*, vol. 58, no. 5, pp. 3469–3483, 2020.

[16] A. M. Molaei, T. Fromenteze, V. Skouroliakou, T. V. Hoang, R. Kumar, V. Fusco, and O. Yurduseven, "Development of fast fourier-compatible image reconstruction for 3d near-field bistatic microwave imaging with dynamic metasurface antennas," *IEEE Transactions on Vehicular Technology*, vol. 71, no. 12, pp. 13077–13090, 2022.

Authorized licensed use limited to: University College London. Downloaded on April 24,2024 at 17:59:49 UTC from IEEE Xplore. Restrictions apply.
© 2024 IEEE. Personal use is permitted, but republication/redistribution requires IEEE permission. See https://www.ieee.org/publications/rights/index.html for more information.

This article has been accepted for publication in IEEE Transactions on Radar Systems. This is the author's version which has not been fully edited and content may change prior to final publication. Citation information: DOI 10.1109/TRS.2024.3387950

[17] H. Hu, D. Zhu, and F. Hu, "A novel imaging method using fractional fourier transform for near-field synthetic aperture radiometer systems," *IEEE Geoscience and Remote Sensing Letters*, vol. 19, pp. 1–5, 2022.
[18] X. Zhuge, A. G. Yarovoy, T. Savelyev, and L. Ligthart, "Modified kirchhoff migration for uwb mimo array-based radar imaging," *IEEE Transactions on Geoscience and Remote Sensing*, vol. 48, no. 6, pp. 2692–2703, 2010.
[19] Z.-Y. Wang, Y. Guo, H. Yang, and Q. Qiu, "A heuristic explanation for the superluminal behaviors of evanescent waves," in *2012 Symposium on Photonics and Optoelectronics*, pp. 1–4, IEEE, 2012.
[20] D. Oloumi and K. Rambabu, "Studying the superluminal behavior of uwb antennas and its effect on near-field imaging," *IEEE Transactions on Antennas and Propagation*, vol. 64, no. 12, pp. 5084–5093, 2016.
[21] S. Schmidt, N. Duric, C. Li, O. Roy, and Z.-F. Huang, "Modification of kirchhoff migration with variable sound speed and attenuation for acoustic imaging of media and application to tomographic imaging of the breast," *Medical physics*, vol. 38, no. 2, pp. 998–1007, 2011.
[22] D. Oloumi, R. S. Winter, A. Kordzadeh, P. Boulanger, and K. Rambabu, "Microwave imaging of breast tumor using time-domain uwb circular-sar technique," *IEEE Transactions on Medical Imaging*, vol. 39, no. 4, pp. 934–943, 2019.
[23] J. M. Lopez-Sanchez and J. Fortuny-Guasch, "3-d radar imaging using range migration techniques," *IEEE Transactions on antennas and propagation*, vol. 48, no. 5, pp. 728–737, 2000.

Authorized licensed use limited to: University College London. Downloaded on April 24,2024 at 17:59:49 UTC from IEEE Xplore. Restrictions apply.
© 2024 IEEE. Personal use is permitted, but republication/redistribution requires IEEE permission. See https://www.ieee.org/publications/rights/index.html for more information.